

## Journal Pre-proofs

pH Activated Colloidal Nanospheres: A Viable Sensing Platform for the Therapeutic Drug Monitoring of the Anticancer Drug 6-Mercaptopurine

Marianna Pannico, Pellegrino Musto

PII: S0169-4332(21)02285-6  
DOI: <https://doi.org/10.1016/j.apsusc.2021.151232>  
Reference: APSUSC 151232

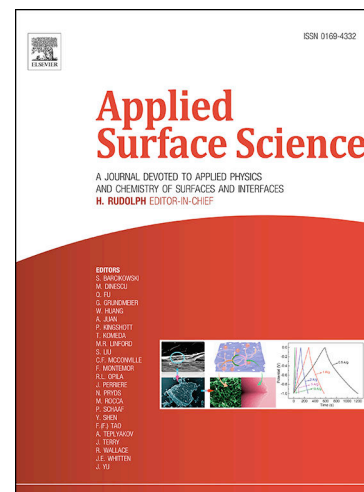
To appear in: *Applied Surface Science*

Received Date: 8 April 2021  
Revised Date: 30 July 2021  
Accepted Date: 6 September 2021

Please cite this article as: M. Pannico, P. Musto, pH Activated Colloidal Nanospheres: A Viable Sensing Platform for the Therapeutic Drug Monitoring of the Anticancer Drug 6-Mercaptopurine, *Applied Surface Science* (2021), doi: <https://doi.org/10.1016/j.apsusc.2021.151232>

This is a PDF file of an article that has undergone enhancements after acceptance, such as the addition of a cover page and metadata, and formatting for readability, but it is not yet the definitive version of record. This version will undergo additional copyediting, typesetting and review before it is published in its final form, but we are providing this version to give early visibility of the article. Please note that, during the production process, errors may be discovered which could affect the content, and all legal disclaimers that apply to the journal pertain.

© 2021 Published by Elsevier B.V.



# **pH Activated Colloidal Nanospheres: A Viable Sensing Platform for the Therapeutic Drug Monitoring of the Anticancer Drug 6-Mercaptopurine**

Marianna Pannico, Pellegrino Musto

National Research Council of Italy, Institute for Polymers, Composites and Biomaterials,  
80078 Pozzuoli (NA), Italy.

**Abstract:** A SERS colloidal solution of gold nanoparticles is proposed as a sensing platform potentially suitable for the Therapeutic Drug Monitoring of the anticancer drug 6-mercaptopurine. The as-synthesized nanospheres were fully characterized in terms of morphological features, plasmonic properties and SERS activity. Modifying the pH of the colloidal solution toward acidic values allowed us to improve considerably the platform sensitivity. A kinetic analysis performed at different analyte concentrations revealed the occurrence of adsorption/aggregation processes which induced a time-dependent SERS response. This dependence, causing unreliable quantitative analysis, was accounted for by a normalizing procedure based on the enhanced elastic scattering signal. After normalization for hot-spot concentration, a 1 – 15  $\mu\text{M}$  linearity range was identified, within which the quantitative analysis is accurate and reproducible. The working range of the present assaying platform is suitable for clinical applications.

**Keywords:** SERS, 6-mercaptopurine, Therapeutic Drug Monitoring, Colloidal solutions, gold nanoparticles, plasmonics

## 1. Introduction

6-mercaptopurine (6-MP) is an active chemotherapeutic agent widely employed as immunosuppressant and in the treatment of acute lymphoblastic leukemia (ALL) [1] and other diseases, such as choriocarcinoma, chorioadenoma, polycythemia, rheumatoid arthritis and inflammatory bowel disease [2]. Together with methotrexate (MTX), 6-MP plays an essential role in the maintenance therapy of ALL in children, [3] whose chemotherapy protocols include daily 6-MP and weekly MTX administration. For 6-MP and related drugs (antiepileptics, anti-HIV agents, anticonvulsants, some antibiotics) for which the therapeutic index is narrow, Therapeutic Drug Monitoring (TDM) is necessary since under-dosage leads to the treatment failure, while serious adverse effects can be caused by overdose [4]. TDM is a clinical practice by which the drug concentration in biological fluids (most commonly, plasma, serum and/or urine) is continuously monitored in order to establish a dosing schedule that would maximize therapeutic results and minimize toxicity [5]. In particular, in cancer therapy TDM has a major impact due to the high cytotoxicity of most anti-cancer agents, which also exhibit a large inter-individual pharmacokinetic variability [6]. In particular, among the pediatric patients this variability is maximized [7]. Current analytical methods for TDM are Gas Chromatography/Mass Spectrometry (GC-MS) and Liquid Chromatography coupled with tandem Mass Spectrometry (HPLC-MS/MS) [8-11]. These are the so-called reference methods and represent the gold standard for TDM in clinical practice. They are robust, relatively free from interference and provide high sensitivity and accurate quantitative results. However, the analyses are costly and require highly trained personnel and expensive infrastructures; as a result, TDM is not practiced routinely in most hospitals, being only available in a limited number of large settings. It is desirable, therefore, to develop alternative analytical approaches for TDM, which could provide a rapid and reliable response with less demanding resources and simpler protocols. Although many techniques (surface plasmon resonance (SPR) [12], electrochemistry [13, 14], voltammetry [15], fluorimetry [16] and spectrophotometry [17] have been proposed for this purpose, they still face numerous problems, especially complex sample preparation and biofouling. One of the techniques currently under consideration for TDM is Surface Enhanced Raman Spectroscopy (SERS) [18, 19]. This spectroscopic tool detects and quantifies analytes in aqueous solution or on suitably fabricated substrates (SERS sensors) in short times (few minutes) and with detection limits and standard errors comparable to or exceeding those of competing analytical methods. SERS consists of the enhancement of the Raman scattering intensity when the analyte is adsorbed on, or in close proximity to nanometer-sized metallic particles. The Raman enhancement occurs primarily by surface plasmon resonance of the exciting laser field and is controlled by the

nanoscale morphology of the metal surface. In optimum conditions, it has been reported that SERS can achieve the single molecule detection limit, which implies a signal increase of up to  $10^{10}$  times with respect to spontaneous emission. More often, the enhancement factor lies in the  $10^5 - 10^7$  range and is well suited for hypersensitive molecular analysis [20, 21]. Moreover, the fingerprinting properties of the Raman spectrum allow the identification of multiple analytical targets in a complex mixture with a single measurement, thus opening up the prospect of multiplex analysis [22]. In addition, peak intensities can provide quantitative estimates of analyte concentration in multicomponent systems. The accuracy and reproducibility of quantitative analysis is a key factor for an assaying method to be appropriate for TDM. In this respect, SERS displays a relevant issue related to the non-uniform response of most sensing platforms. The underlying reason for this unpredictable behaviour originates from the complex interplay of molecular events at the core of the SERS effect, namely the adsorption of the analyte on the sensing surface and the aggregation/precipitation processes in the case of colloidal solutions and the uneven distribution of nanoparticles and *hot-spots* in the case of 2-D solid substrates. Thus, compared to the substantial number of literature studies aimed at exploiting SERS sensitivity, relatively few papers have been devoted to the application of this spectroscopic tool to quantitative analysis [23].

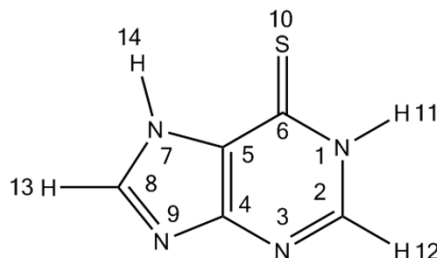
6-MP is well suited for SERS detection because of the reactivity of its various functional groups towards coinage metals. In the present contribution, we focused our attention to the analytical application of AuNPs colloids for 6-MP detection in TDM practice. We synthesized gold nanoparticles with a specific size and shape by the seed-mediated growth method. Once prepared, the colloidal AuNPs were fully characterized in terms of morphological features, plasmonic properties and SERS performance. Then, the sensitivity of the proposed SERS platform was improved by adjusting the pH, and the complex kinetic behaviour of the system was investigated to gather information on the occurring adsorption/aggregation processes. The study allowed us to confirm the proposed SERS platform as a perspective route to TDM and to identify the limit of detection and a highly linearity range for a reliable quantitation of the target analyte.

## 2. Experimental section

### 2.1. Materials

6-mercaptapurine (6-MP, molecular formula in scheme 1), Trisodium citrate (TC), gold (III) chloride trihydrate ( $\text{HAuCl}_4 \cdot 3\text{H}_2\text{O}$ ), ascorbic acid (AA), sodium borohydride ( $\text{NaBH}_4$ ), Cetyltrimethylammonium bromide (CTAB), ethanol, p-Mercaptoaniline (pMA) and hydrochloric

acid (HCl) were reagent-grade products from Sigma-Aldrich and were used as received. Milli-Q (MQ) water was used for the synthesis of gold nanoparticles and for the preparation of all 6-MP solutions.



**Scheme 1.** Molecular formula of 6-MP (N7H thione form) with atom numbering.

## 2.2. Synthesis of gold nanoparticles

The gold nanoparticles (AuNPs) were synthesized in aqueous solution by using the seed-mediated growth method as described in our previous work [24]. Briefly, a seeds (~3 nm) solution was prepared at room temperature by dissolving a prescribed amount of the gold salt and TC in water to get a final concentration  $2.5 \times 10^{-4}$  M of both reagents. Then, under stirring, 600  $\mu$ L of ice-cold  $\text{NaBH}_4$  aqueous solution (0.1 M) were added and the color immediately turned pink, characteristic of seeds formation. The prepared solution was left undisturbed at room temperature for 2 hours and then used for particles growth. Next, a growth solution (GS) was prepared by adding CTAB (final concentration 0.08 M) to a water solution containing  $2.5 \times 10^{-3}$  M of  $\text{HAuCl}_4$ . The mixture was heated at around  $80^\circ\text{C}$  till it turned clear orange and then it was cooled down to room temperature before use. For the nanoparticles growth, 1.0 mL of 0.1 M AA aqueous solution and the seed solution were added to GS which immediately turned wine red color indicative of nanoparticles formation. The solution was stirred for 10 minutes and then centrifuged three times at 13,000 rpm,  $35^\circ\text{C}$  for 15 minutes. The AuNPs were resuspended in water and kept at room temperature for further characterization.

## 2.3. Functionalization of the gold nanoparticles

After centrifugation and re-dispersion in water, the gold nanoparticles were functionalized with pMA to test their SERS performance. A 100  $\mu$ M ethanol solution of pMA was added to the AuNPs colloidal solution (v/v 1:1) and stirred at room temperature for 10 minutes. Gold nanoparticles were functionalized with 6-MP as follows: a water stock solution of 6-MP (1.0 mM) was prepared and used to get diluted 6-MP solutions ranging from 20 to 0.1  $\mu$ M. Equal volumes of 6-MPs and AuNPs

solutions (v/v 1:1) were mixed and stirred at room temperature for a fixed time. To test the effect of pH on the SERS intensity, HCl 1.18 M was added to the 6-MP functionalized nanoparticles solutions (colloidal solution /HCl, 5:1 v/v).

## 2.4. Techniques

### 2.4.1. UV-VIS spectroscopy

The optical properties of AuNPs and their molar concentration were measured by an UV spectrophotometer equipped with a single monochromator (V-570 from Jasco, Easton, USA). Absorption spectra of the AuNPs colloids were collected using 1.00 cm quartz cell with a scan speed of 400 nm/min in the wavelength range from 300 to 800 nm. For the quantitative analysis of the gold amount in the AuNPs solution a set of six standards were obtained by diluting the as-prepared AuNP solution batch. Complete reduction from Au(III) to Au(0) was assumed.

### 2.4.2. Transmission electron microscopy (TEM)

The AuNPs morphology, size and shape were examined by bright field transmission electron microscopy, performed on a FEI Tecnai G12 Spirit Twin (LaB6 source) equipped with a FEI Eagle 4 K CCD camera (Eindhoven, The Netherlands) operating with an acceleration voltage of 120 kV. Samples for TEM examination were prepared by immersing a carbon-coated copper grid in the colloidal solution, and drying at ambient conditions. At least 10 TEM images were acquired in different sample areas and were used for the Statistical Image Analysis (SIA), performed by the PLS/MIA software package (Eigenvector Research Inc., Manson, WA, USA) running under the MATLAB computational platform (Mathworks, Natick, MA, USA).

### 2.4.3. Raman Spectroscopy

The Raman spectra were collected by a confocal Raman micro spectrometer (XploRA, Horiba-Scientific, France) with a 638 nm diode laser as exciting source and an Edge filter for collecting the Stokes scattering down to  $50\text{ cm}^{-1}$ . The radiation was collected by an Olympus metallurgical objective (MPlan 10x, NA = 0.25 or 50x, NA = 0.50, depending on the sample) with confocal and slit apertures set to 500 and 200  $\mu\text{m}$ , respectively. A grating with 600 grooves/mm was used to disperse the scattered light. The pMA reference spectrum was collected in solution (10 wt% in ethanol) by a 10x/0.25 objective and 10 seconds of exposure time. The pMA and 6-MP SERS spectra were collected in solution with a 10x/0.25 objective using a quartz cuvette with chamber volume of 700

$\mu\text{L}$  (Hellma GmbH & Co, Jena, Germany). The acquisition time was selected depending on sample response. The chosen instrumental parameters allowed for an optimum signal-to-noise ratio (SNR), exceeding 24 for a 6-MP solution at the lower boundary of the dilution range (1.0  $\mu\text{M}$ ).

Kinetic experiments in acidic condition were carried out in solution by off-line measurements. In a quartz cuvette, a 6-MP water solution was added to an AuNPs colloidal solution in a 1:1 volume ratio; then HCl 1.8 M was added in a 5:1 volume ratio with respect to the colloidal solution. Right after the reagents mixing, the cuvette was transferred to a mechanical shaker for continuous stirring. At prescribed times the cuvette was moved to the Raman spectrometer for recording the SERS spectra, and quickly returned to the shaker. A 10x/0.25 objective was used throughout. Two 6-MP concentrations, 5 and 20  $\mu\text{M}$ , were tested. The raw spectral data were converted into ASCII format and transferred to the MATLAB computational platform for further processing.

### 3. Results and discussion

#### 3.1. Transmission Electron Microscopy

Fig. 1A displays a typical TEM micrograph taken on the pristine colloidal solution (pH = 3.50). Ten of these images, providing a total nanoparticle population of  $\cong 800$  units, were employed to perform a Statistical Image Analysis (SIA, Fig. 1B). According to our previous work [24] the shape and shape distribution of the AuNPs were evaluated by means of the Roundness parameter, defined as:

$$R = \frac{4 \times A}{\pi \times d_{max}^2} \quad (1)$$

where  $A$  is the particle area and  $d_{max}$  is the major axis. It was found that 98% of the NPs had a spherical shape (roundness  $\geq 0.85$ ), with an average diameter of  $16 \pm 2.5$  nm. The size-distribution of the particles is sharp and has a gaussian-like shape, as generally observed in the absence of multimodal distribution. Less than 2% of the total nanoparticles had an  $R$  value lower than 0.6, indicative of a rod-like shape. In the whole set of TEM images, no evidence of particle aggregation was found, confirming that the CTAB bilayer surrounding the nanosphere effectively inhibits aggregation through repulsive electrostatic interactions among AuNPs. The micrograph in Fig.1C was collected on the AuNPs solution after injection of a 10  $\mu\text{M}$  solution of 6-MP (pH = 4.5). Previous studies demonstrated that, in these conditions, the substitution of the initial CTAB bilayer with a 6-MP monolayer is essentially complete.

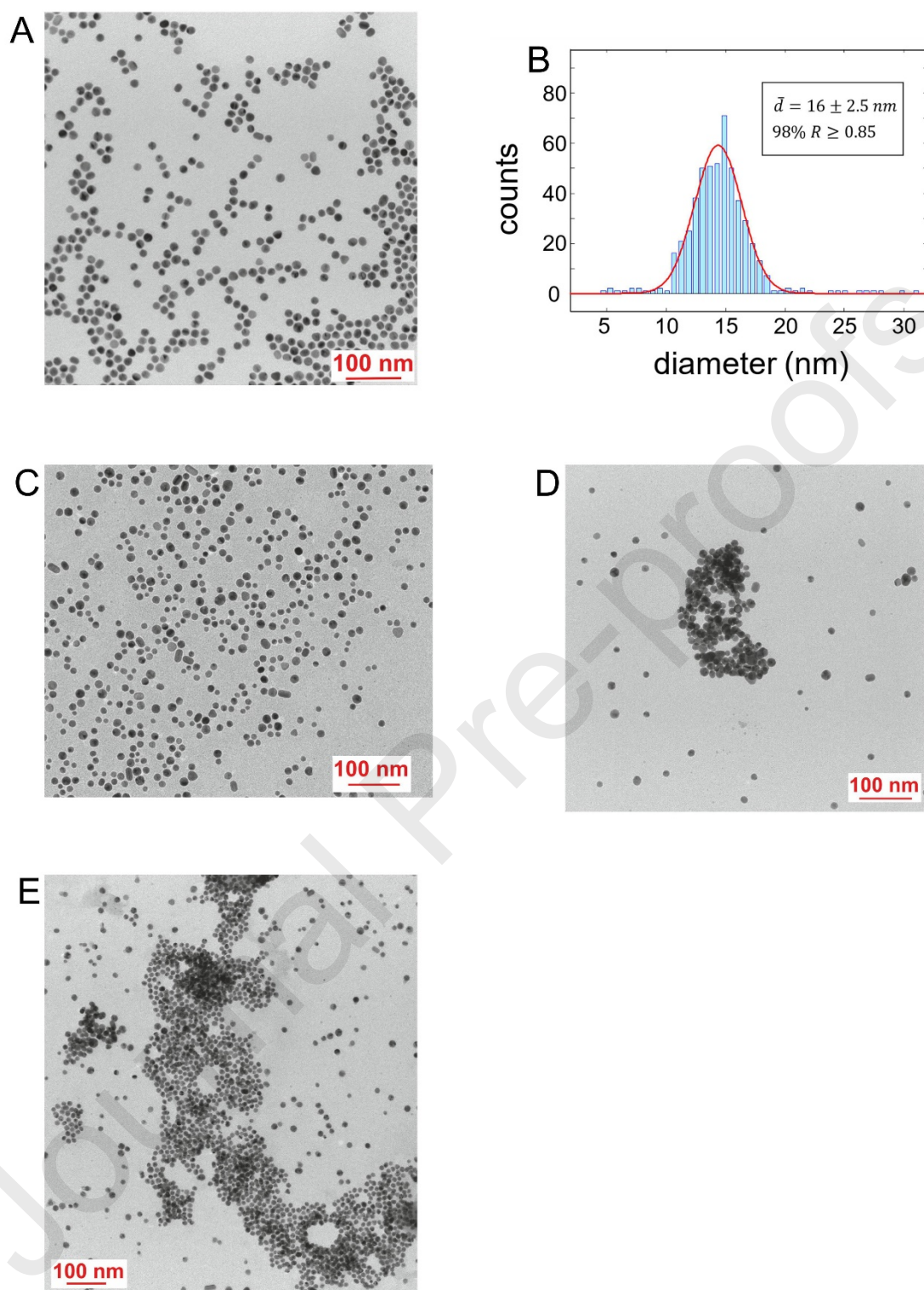


**Figure 1.** TEM micrographs and SIA analysis of AuNPs colloidal solutions. A) TEM of the pristine colloid (pH = 3.50); B) SIA analysis of the pristine colloid; C) TEM of the AuNPs colloidal solution additivated with a 10  $\mu\text{M}$  solution of 6-MP (pH = 4.5). D) The above solution acidified at pH = 0.17; TEM analysis performed after 10 min from acidification. E) As above, TEM analysis after 3 h from acidification.



SIA analysis showed no significant changes with respect to the pristine colloid, indicating that the neutral surface charge of the nanoparticles after 6-MP adsorption still provides a stabilizing condition against aggregation. It is known that the ionic strength of the solution plays a key role in colloidal stability. In fact, by shifting the pH of the considered AuNPs/6-MP solution from the initial value of 4.5 to highly acidic values, we clearly observed the onset of AuNPs coalescence. Fig. 1D represents the AuNPs/6-MP solution activated by HCl at pH = 0.17 after 10 min from the addition of HCl: numerous aggregates are present, which coexist with isolated nanoparticles. The aggregate in Fig. 1D, with  $d_{max} = 295$  nm and an aspect ratio of 1.9, is among the largest observed under these conditions. TEM analysis of the same solution after 3 hours (*cf* Fig. 1E) shows extensive coalescence, with aggregates extending over the whole image field. These domains are likely to precipitate from the supernatant solution at longer times.

### 3.2. Plasmonic properties

The pristine AuNPs exhibit a localized surface plasmon resonance (LSPR) band at 523 nm, with a narrow shape that, according to the SI analysis, is indicative of a unimodal distribution of nanoparticle dimensions (*cf* UV-VIS spectrum in Figure S1, supplementary data). The spectrum is only slightly affected after AuNPs functionalization with 6-MP (a red-shift of 1.0 nm, see Fig. 1S, Supplementary Material) confirming that the plasmonic properties of the nanosphere are marginally affected by the surface layer, and are controlled essentially by its dimensions. The UV-VIS spectrum was used to evaluate the gold molar concentration in the colloid solution taking advantage of the Beer-Lambert behaviour of the system (*cf* Fig. S2, Supplementary Material data). According to our previous work [24] by coupling the TEM geometrical parameters (size and shape) and the UV-VIS results ( $[Au]$ ) the calculated AuNPs concentration was 21.0 nM. The SERS activity of the synthesized colloids was quantified by measuring the absolute enhancement factor ( $EF$ ), i.e. by comparing the SERS response of a reference analyte (p-mercaptoaniline, pMA) with its spontaneous inelastic scattering. [25]. The  $EF$  was calculated according to the procedure reported in [24]. Its value,  $3,0 \times 10^5$ , was found suitable for high-sensitive analytical applications of SERS spectroscopy [22, 25].

### 3.2. The colloidal solution as SERS sensor for 6-MP detection.

The adsorption of 6-MP on a colloidal solution of gold nanospheres was investigated in detail in a previous contribution of this series [26]. Accuracy/precision appropriate for TDM analysis were achieved at the expenses of sensitivity by limiting aggregation phenomena. In the light of the above results, we adopted the alternative approach of modifying the ionic strength of the solution so as to

induce the formation of stable nanosphere assemblies with an adequate *hot-spot* density to boost SERS activity. The approach is demonstrated in Fig. 2, in which are compared the SERS spectra of the AuNPs (21.0 nM)/6-MP 20  $\mu$ M solutions with different acidity. In particular, the red trace refers to the plain solution (pH = 4.5) while the blue trace is relative to the solution activated by HCl to reach a pH value of 0.17 (see experimental). Both spectra were collected after 180 min from the analyte injection, maintaining the solution under mild mechanical stirring. The dramatic increment of the signals intensity confirms the strong influence of the medium acidity on SERS activity. In agreement to the results of the TEM analysis, the effect is ascribed to an aggregation process triggered at low pH values rather than an increase of adsorption efficiency of 6-MP species prevailing in the acidic environment. In fact, previous results indicated a very high affinity of the target molecule towards the metal surface even at moderate/neutral pH values.[26, 27].

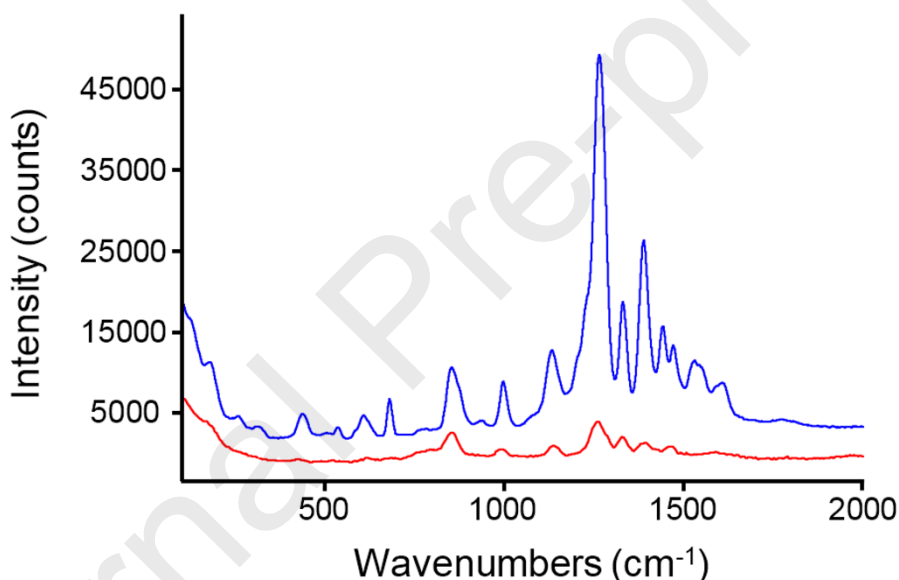


**Figure 2.** Red trace: SERS spectrum of the AuNPs/6-MP 20  $\mu$ M solution at pH = 4.5. Blue trace: The above solution activated by HCl (pH = 0.17). Spectra collected after 270 min from analyte injection.

Fig. 2 demonstrates that, activating the colloidal solution by acidification, increases the sensitivity by one order of magnitude, as evaluated from the intensity ratio of the strongest peak at 1259  $\text{cm}^{-1}$  ( $I''_{1259}/I'_{1259} = 9.93$ , where primed and double primed symbols refer, respectively, to the plain and the acidified solutions). The blue-trace spectrum in Fig. 2 is consistent with earlier literature reports on SERS spectra of 6-MP in acidic media [26, 28-30]. These were recently interpreted on the basis of a Quantum Mechanical (*QM*) vibrational analysis, which provided molecular-level insight in the interaction mechanism and the adsorbate orientation [26]. It was found that 6-PM assumes a flat orientation with respect to the colloid surface and the binding mechanism involves covalent bonding

(formation of a gold thiolate species) plus non-covalent interactions with the N1/N7 atoms and the pyrimidine  $\pi$  cloud. Non-covalent interactions represent the primary contribution stabilizing the flat orientation. The *QM* analysis afforded the evaluation of the molecular cross-section of 6-PM ( $65 \text{ \AA}^2$ ), which, coupled with the geometric parameters of the colloid, revealed that a maximum of 1237 molecules can be adsorbed on a single NP. It was inferred that the colloid saturation is reached at a 6-MP concentration of  $26 \text{ \mu M}$  in the conditions of the present study [26]. Several peaks display a consistent bandshape over the considered concentration range, a well defined baseline and are fully resolved, which makes them suitable for quantitative analysis (*cf* also Figs. S3 and S5, Supplementary Material). They occur at  $671 \text{ cm}^{-1}$  [ $\nu(\text{N3C4}) / \delta(\text{C4N9C8})$ ],  $991 \text{ cm}^{-1}$  [ $\delta(\text{N7C8N9}) / \delta(\text{C4N9C8})$ ],  $1126 \text{ cm}^{-1}$  [ $\nu(\text{N7C8}) / \nu(\text{N1C2}) / \delta(\text{H14N7C8})$ ],  $1323 \text{ cm}^{-1}$  [ $\nu(\text{N3C4}) / \delta(\text{H13C8N9})$ ] and  $1380 \text{ cm}^{-1}$  [ $\nu(\text{N7C8}) / \nu(\text{N9C4}) / \delta(\text{C5N7C8})$ ] [26]. In the above notation the Greek letters have the usual meaning of stretching ( $\nu$ ) and in-plane bending ( $\delta$ ) and atom numbering refers to Scheme 1. The intense peak at  $1259 \text{ cm}^{-1}$  is useful to test the limiting sensitivity due to its substantial Raman cross-section, but is less effective for quantitative analysis because of a complex bandshape changing significantly with 6-MP concentration.

We observed a pronounced variability of the SERS response with time at all investigated compositions. This effect is highlighted in Fig. 3, where the bar-graph represents the intensity of the  $1380 \text{ cm}^{-1}$  peak in the considered solutions at given time intervals.

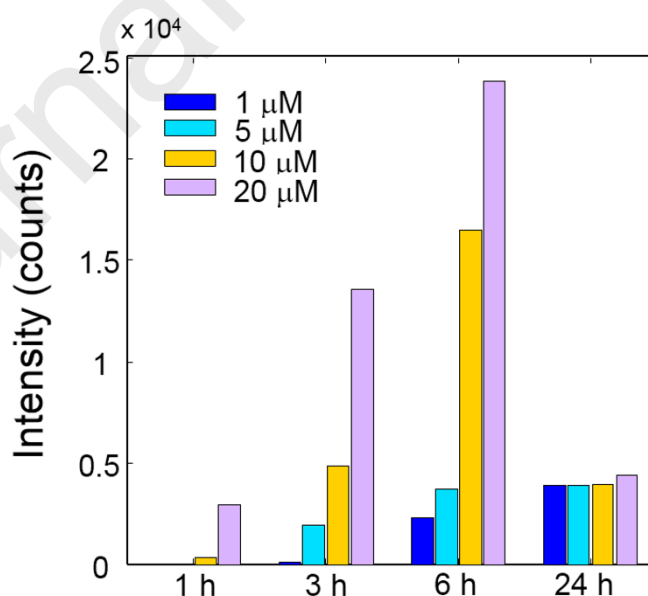


**Figure 3.** Intensity of the SERS signal at  $1380 \text{ cm}^{-1}$  at given time intervals for different 6-MP solutions. Concentrations as indicated.

For the 1  $\mu\text{M}$  composition, the SERS intensity is barely detectable in the first 3 h, but emerges clearly after 6 h and increases slightly after 24 h. The 5  $\mu\text{M}$  composition shows an analogous behaviour, except that the signal intensity is already obvious after 3 h. At 10 and 20  $\mu\text{M}$ , the SERS activity is substantial from the very beginning and keeps growing in the following six hours. Interestingly, all considered compositions display very close values of SERS intensity in the long-term (24 h) collection. It is clear that the kinetic behavior of the system is complex and has a profound effect on both the sensitivity and the accuracy of the proposed platform. For instance, at 1  $\mu\text{M}$  the sensitivity boosts by a factor of 15.4 in the first six hours, while at 20  $\mu\text{M}$  increases 8.1 times. No obvious correlation between SERS activity and analyte concentration emerges at this stage. Identifying composition ranges and protocols for quantitative analysis demands an accurate characterization of the kinetic behaviour. To this end, we analyzed in detail the 20 and the 5  $\mu\text{M}$  compositions, whose results are reported, respectively, in Figs. 4 and 6.

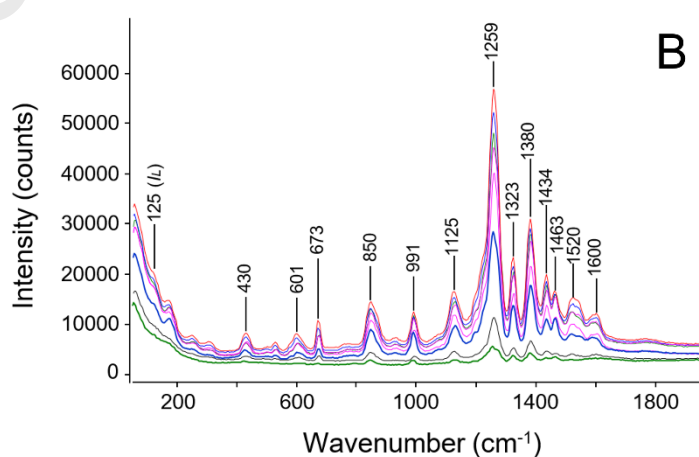
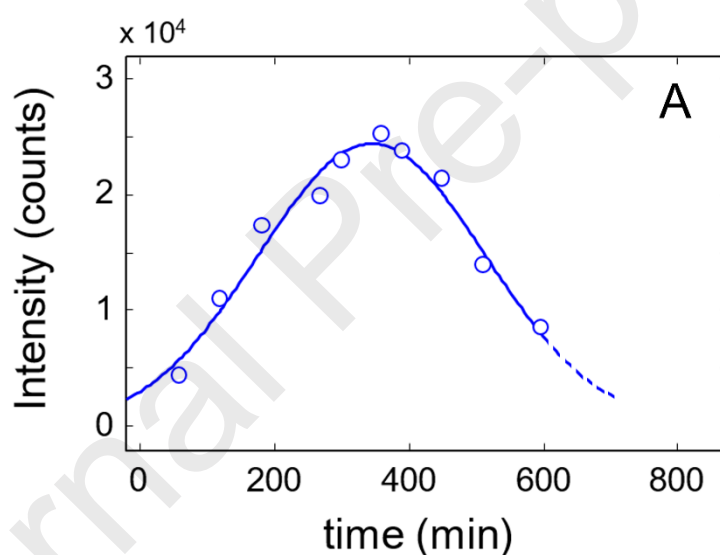


**Figure 4.** A) Time evolution of the SERS signal at  $1380\text{ cm}^{-1}$  in the colloidal solution after injection of a  $20\text{ }\mu\text{M}$  solution of 6-MP and activation by HCl ( $\text{pH} = 0.17$ ). B) SERS spectra collected at different times. Black trace: 60 min; purple: 150 min; brown: 180 min; green: 270 min; blue: 360 min; red: 390 min; dark blue: 510 min; green: 1440 min.

The  $20\text{ }\mu\text{M}$  solution displays an initial fast-growing regime that reaches a maximum at 380 min. Afterwards the SERS activity starts to decline with a rate comparable to that of the initial growth. After 700 min the intensity of the analytical peak approaches the  $t_0$  value. The adsorption kinetics of numerous analytes on gold and silver surfaces has been investigated [31, 32]. In particular, it was shown that aromatic thiols follow a first-order Langmuir adsorption model with kinetic constants at ambient temperature of the order of  $0.01\text{ min}^{-1}$ , which allows to reach equilibrium within 200 – 300 min under experimental condition close to those of the present study. Thus, the results of Fig. 4A are compatible with an adsorption process ruled by a Langmuir mechanism. However, the observation of a well-detectable SERS signal at  $t_0$  conflicts with this hypothesis. A sounder scenario is the instantaneous (in the time-scale of the experiment) adsorption of the probe onto the available metal surface, followed by a much slower aggregation process triggered by the simultaneous effect of the modified surface charge and the ionic strength of the solution. This interpretation is supported by the results of the TEM analysis. Thus, responsible for the signal increase in the initial regime is the formation of hot-spots within the nanoparticle aggregates, which is likely to induce a complex dependence of the SERS intensity on analyte concentration, that is, a pronounced non-linearity of the response function. A very fast adsorption rate of 6-MP as compared to aromatic thiols has been already postulated in Refs [26, 27] and can be justified considering the numerous functional groups present in the 6-MP molecule and their pronounced affinity towards the Au surface. The exponential-decay regime following the maximum at 360 min is due to the formation of aggregates that have reached a critical size for inducing precipitation and consequent loss of SERS activity from the solution. The kinetic analysis indicates that substantial precipitation of AuNPs occurs after 600 min.

Further experimental evidence of the above interpretation is provided by the UV-Vis spectra collected on the  $20\text{ }\mu\text{M}$  solution as a function of time (see Fig. 5). The LSPR band at 524 nm observed at time zero evolves into a more complex profile at 300 min. In particular, the main component red-shifts by 12 nm and a second band approximately centred at 665 nm emerges. These features represent the characteristic signature of colloid aggregation [33]. At longer times, the band intensity gradually weakens, becoming barely detectable at 800 min, which confirms the progressive precipitation of the aggregates.

The extensive aggregation induced by HCl addition is to be related to the acid-base properties of 6-MP. This conclusion is supported by the observation that, adding HCl to the pristine AuNPs solution in the same concentration ratio used to activate the 6-MP solutions produces a very limited aggregation (*vide infra*). The acid-base behavior of free 6-MP is intricate, and is further complicated by the existence of different tautomeric species in solution. It has been shown, however, that the molecule is protonated at the N(1) position in a strong acidic medium [27] and the same behaviour is likely for the molecule adsorbed on the gold surface. One possible interpretation is that postulated in Ref [27], i.e. the protonation may contribute to strengthen the intermolecular interactions typically active in these nucleobase analogues (base stacking interactions). Those established between molecules residing on adjacent nanoparticles compensate for residual electrostatic repulsion and trigger aggregation.

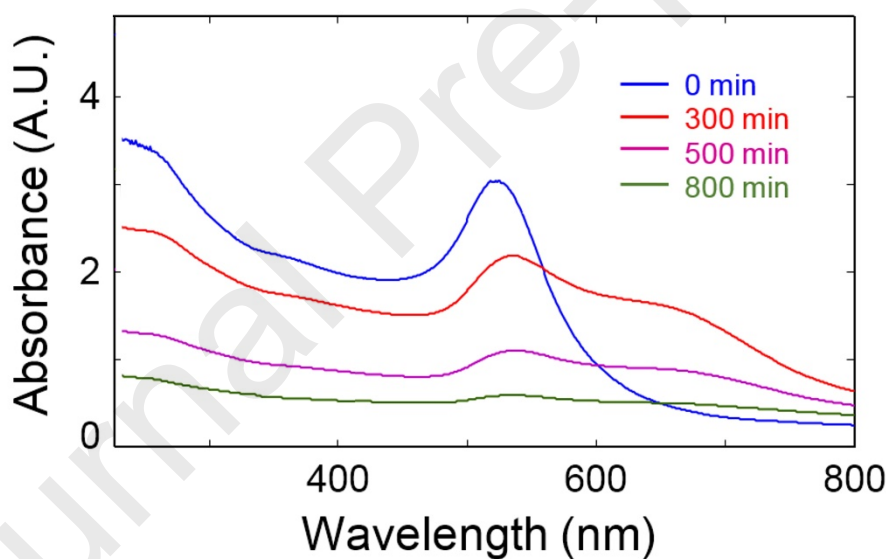


**Figure 5.** UV-Vis spectra collected at different times on the colloidal solution after injection of a 20  $\mu\text{M}$  solution of 6-MP and activation by HCl ( $\text{pH} = 0.17$ ). Collection times as indicated.

Similar arguments can be put forward to explain the time evolution of the SERS activity for the 5  $\mu\text{M}$  solution. At this composition precipitation is very slow compared to the initial formation of the primary AuNPs aggregates. In fact, the latter process lasts around 500 min, while the former is more than one-order of magnitude longer. A further observation is the occurrence of an induction period of around two hours prior to the increasing regime (see inset of Fig. 6), likely due to the time required

to reach a detectable amount of *hot-spots* in the given conditions of mixing and NPs concentration. The weak and constant intensity detected in this interval (480 counts/s) represents, therefore, the SERS activity of the isolated nanospheres, i.e. the single-particle regime. Its value compares favourably with that reported in Ref. [26], thus confirming that the probe adsorption is essentially instantaneous and the time dependence of the SERS activity is solely due to aggregation/precipitation processes.

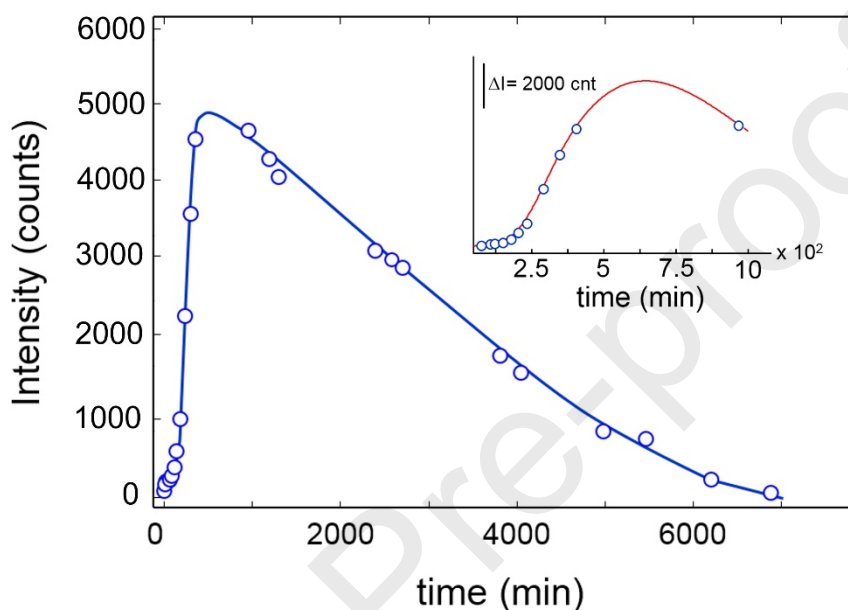


**Figure 6.** Time evolution of the SERS signal at  $1380\text{ cm}^{-1}$  in the colloidal solution after injection of a  $5\ \mu\text{M}$  solution of 6-MP and activation by HCl ( $\text{pH} = 0.17$ ).

The kinetic analysis discussed so far reveals that adjusting the ionic strength of the solution is an effective means for improving the sensitivity but induces side-effects (especially precipitation) which cause an unwanted time-dependence of the SERS signaling. However, the kinetics of the underlying processes is slow compared to the time-scale of the experiment, suggesting that it could be possible to identify a set of conditions to get a SERS response which is stable both spatially and temporally, and could be usefully correlated with the analyte concentration.

### 3.3. Quantitative analysis enabled by surface enhanced elastic scattering

As already mentioned, a primary requirement for an assaying method to be useful in TDM is the accuracy and reproducibility of the quantitative analysis. The strong time-dependence of the present platform in terms of SERS activity makes it difficult to envisage a protocol that could maximize sensitivity while ensuring a linear response toward analyte concentration. In the preceding section we

have shown that the increment of SERS signaling in the colloidal solution is due to *hot-spots* formation (NPs aggregation), while the signal lowering is caused by loss of *hot-spots* (NPs precipitation). Therefore, a suitable strategy towards SERS quantitation would be to normalize the analyte signal over *hot-spot* concentration within a given time interval. It has been recently demonstrated that a given *hot-spot* produces the same electromagnetic enhancement on both the elastic and the inelastic (Raman) scattering [34, 35]. Based on these studies, a suitably chosen surface-enhanced elastic scattering signal can be tested as a localized intrinsic internal standard that scales across all of the plasmon-enhanced electromagnetic fields within a substrate. In a Raman/SERS experiment, the elastically scattered light is removed by an edge or a notch filter, depending on instrument configuration, to avoid interference and detector saturation. It produces a sharp spike around the *zero* value of the Raman-shift and goes undetected. However, commercial lasers, besides emitting at the fundamental frequency,  $\omega_0$ , also radiate parasitic light at close frequency ( $\omega_1$ ), with an intensity that is orders of magnitude lower than the primary emission. The elastically scattered radiation originating from this secondary spontaneous emission is actually detectable because of the combined effect of the frequency shift and the reduced intensity with respect to the fundamental. It gives rise to the formation of a low-wavenumber pseudo-band in the vicinity of the filter cut-off. According to Wei and co-workers [36] the ratio between the intensities of the Raman and the elastic signals ( $I_R$  and  $I_{El}$ , respectively) can be approximated as:

$$\frac{I_R(\omega_0 \pm \omega_{vib})}{I_{El}(\omega_1)} \approx \frac{N_A |\alpha_A(\omega_0 \pm \omega_{vib}, \omega_0)|^2 I_0(r_0, \omega_0)}{N_B |\alpha_B(\omega_1)|^2 I_0(r_0, \omega_1)} \quad (2)$$

In eq. 2  $\omega_0$ ,  $\omega_1$  and  $\omega_{vib}$  are, respectively, the lasing frequency, the secondary emission frequency of the laser source and the vibrationally shifted frequency;  $\alpha_A$  and  $\alpha_B$  are, respectively, the Raman scattering polarizability of the analyte molecules and the elastic scattering polarizability of the background molecules;  $N_A$  and  $N_B$  are the molar concentrations of the analyte and the background solvent molecules present within the sampling volume ( $N_B \gg N_A$ );  $I_0$  is the incident field intensity and  $r_0$  is the position of the molecule under plasmonic resonance. During a SERS measurement, all factors in eq. 2 (i.e.,  $N_B, \alpha_A, \alpha_B, I_0(r_0, \omega_0)/I_0(r_0, \omega_1)$ ) are constant except  $N_A$ . This implies that, by normalizing the SERS signals with the surface-enhanced elastic scattering signals of the background molecules in the *hot spots*, the ratiometric value in the left side of eq.2 provides a quantitative estimate of the molar concentration of the analyte which is unaffected by the numerous factors generating the unpredictable spatial and temporal perturbations of the SERS intensity. The situation is represented



in Figs. S3, Supplementary Material, and in the lower wavenumber side of Fig.4B. In Fig. S3A are compared the spectra collected in the absence of AuNPs (MQ water, blue trace), in the pristine colloidal solution prior to 6-MP addition (red trace) and in the colloidal solution brought in contact with 20  $\mu\text{M}$  of 6-MP and activated by HCl addition (purple trace). The low-frequency pseudo band is weak in pure water, reflecting the absence of any enhancement mechanism. It remains essentially the same when the AuNPs do not aggregate, indicating that, without hot-spots, which are formed to a significant extent only after activation (see TEM micrographs in Figs. 1), the isolated nanospheres do not provide an appreciable enhancement effect. The elastic scattering intensity increases substantially when the aggregation process is triggered by adding 6-MP and acidifying the solution (*cf* Fig.S3A, purple trace). The gradual increase of the elastic scattering pseudo-band with *hot-spots* concentration is also apparent in Fig. 4B. Fig. 7 illustrates the relationship between  $I_{EL}$  and the 6-MP SERS spectrum above 400  $\text{cm}^{-1}$  for the data set represented in Fig. 4 (20  $\mu\text{M}$  solution). The overall amount of elastic scattering has been evaluated by integrating the Intensity vs frequency profile in the 50 – 350  $\text{cm}^{-1}$  range, while the total SERS activity (inelastic scattering) is the area within the 375 – 1750  $\text{cm}^{-1}$  range. The excellent linear correlation between the two plasmonically-enhanced scattering phenomena ( $R^2 = 0.965$ ), evaluated considering the whole contribution in the respective frequency intervals, confirms the premise that a *hot-spot* produces the same effect on elastic and inelastic scattering, and that eq. 2 can be reliably employed for normalization purposes [34, 35].

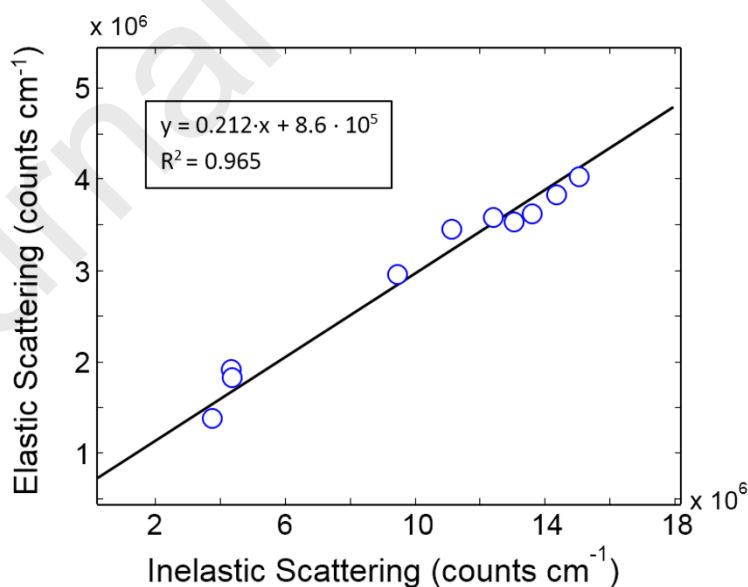


**Figure 7.** Elastic scattering as evaluated from the area under the spectrum in the 350 – 50  $\text{cm}^{-1}$  range, and the inelastic scattering (area in the 1750 – 375  $\text{cm}^{-1}$  range). Data collected at different times on the colloidal solution with 20  $\mu\text{M}$  of 6-MP activated by HCl ( $\text{pH} = 0.17$ ).

We explicitly note that the development of an intense SERS pattern is accompanied by the appearance of a broad background diffusion with a maximum at  $\approx 1400 \text{ cm}^{-1}$  (*cf* Figs. 3SA – 3SB, Supplementary Material). This effect is also due to a plasmon-activated process and, in particular, to photoluminescence [36]. In fact, in Fig. 4B the background level is found to increase gradually with SERS activity, confirming the common physical origin of the two processes. In principle, photoluminescence could provide an alternative normalizing signal, but attempts in this direction were unsuccessful [36] likely because of the extreme breadth and ill-defined shape of the band. Thus, in the present data treatment, the effect of photoluminescence has been compensated for by a proper baseline correction (*cf* Fig. S3B). In Ref [36] the quantitative estimation of the elastic scattering intensity was made by integrating the band between 106 to  $146 \text{ cm}^{-1}$ ; in our case we preferred to work with peak heights, because the analytical signals are well resolved and peak heights are less sensitive than areas to baseline fluctuations. Thus, for dimensional consistency, we adopted as the normalizing factor ( $I_{El}$  in eq. 2) the intensity value at  $126 \text{ cm}^{-1}$  ( $I_{126}$ ).  $I_{126}$  was found to be linearly related to the overall amount of elastic scattering represented in Fig. 7.

To confirm the soundness of the proposed normalizing approach we have investigated the possible influence of the  $\text{Cl}^-$  ion in the frequency range of interest. In fact, it has been reported [37, 38] that, in certain conditions,  $\text{Cl}^-$  ions are adsorbed on the AuNPs and produce SERS signals in the  $100 - 300 \text{ cm}^{-1}$  range. In particular, in Ref. 37  $\text{Cl}^-$  adsorption was observed on a  $15 \mu\text{M}$  colloidal solution of nanospheres having a  $15 \text{ nm}$  diameter, stabilized by a citrate coating. A doublet was detected at  $130 - 240 \text{ cm}^{-1}$ : the high frequency component was assigned to  $\nu(\text{Cl}-\text{Au})$  vibration, while the origin of the low-frequency peak remained undefined. It was found that isolated nanoparticles produced relatively weak SERS signals but, on aggregation of the cit-AuNPs, the SERS intensity grew. Measurements at increasing times showed the intensity enhancement of the SERS signals, ascribed to the formation of *hot-spots*. The aggregation was attributed to the combined effect of citrate substitution by  $\text{Cl}^-$  and the destabilizing effects of the sodium ion.

We added HCl to the pristine AuNPs colloidal solution in the same concentration ratio used to activate the 6-MP solutions (see Experimental). The SERS spectra in the  $100 - 500 \text{ cm}^{-1}$  range of the resulting colloid collected at increasing times from HCl addition are reported in Fig. S4, Supplementary Material. At time zero the profile is essentially featureless, but after 180 min, a well resolved, highly symmetrical peak emerges at  $185 \text{ cm}^{-1}$ . By comparison with the spectra reported in [37] we assign this feature to the  $\nu(\text{Au}-\text{Cl})$  mode enhanced by SERS. This observation confirms that HCl is able to adsorb on AuNPs, displacing the preexisting CTAB bilayer, as it does with the citrate monolayer

[39]. The  $\nu(\text{Au}-\text{Cl})$  vibration is readily recognized due to its sharp contour and does not interfere with the broad, underlying background emission, as demonstrated by a curve fitting analysis. The spectrum collected after 570 min displays a minimal enhancement, possibly reflecting a small amount of *hot-spot* formation as a consequence of NPs aggregation, as suggested in [37]. The effect is negligible with respect to those observed on the colloids functionalized with 6-MP, confirming that extensive AuNPs aggregation is triggered by the presence of the 6-MP functional groups on the metal surface. In Fig. S4, Supplementary Material, are reported the SERS spectra of the AuNPs colloidal solution functionalized by a 5  $\mu\text{M}$  solution of 6-MP and activated by HCl. The sequence of spectra was collected at increasing times after 6-MP injection. The 185  $\text{cm}^{-1}$  peak is clearly discerned and is found to increase with time, which indicates that  $\text{Cl}^-$  is adsorbed even in the presence of 6-MP. However,  $\text{Cl}^-$  is able to displace only the CTAB bilayer, while leaving the strongly interacting 6-MP intact, as demonstrated by the intense SERS signaling of the latter.  $\text{Cl}^-$  adsorption occurs at this composition because of the excess of available adsorption sites over the amount of analyte. According to the structural data reported in Ref. [26], at 5  $\mu\text{M}$  concentration the surface coverage by 6-MP amounts to 28 %, assuming full yield of the 6-MP adsorption process.

At 20  $\mu\text{M}$  composition (cf in Fig. 4B and Fig. S6, Supplementary Material) the 185  $\text{cm}^{-1}$  peak is barely detectable. This is because at this composition the surface coverage by 6-MP is almost complete (saturation threshold calculated at 26  $\mu\text{M}$ ). In general, the presence of 6-MP tends to hinder  $\text{Cl}^-$  adsorption even at intermediate compositions when the surface coverage is incomplete. In fact, the 185  $\text{cm}^{-1}$  signal is evident only at 5  $\mu\text{M}$ , while becoming very weak with respect to the underlying background, at any other investigated composition. This analysis demonstrates that, even if  $\text{Cl}^-$  can adsorb on AuNPs residual sites (e.g. those not occupied by 6-MP), its interference on the elastic scattering pattern employed to normalize for *hot-spot* concentration, can be considered negligible. This conclusion is corroborated by the linear relationship reported in Fig. 6.

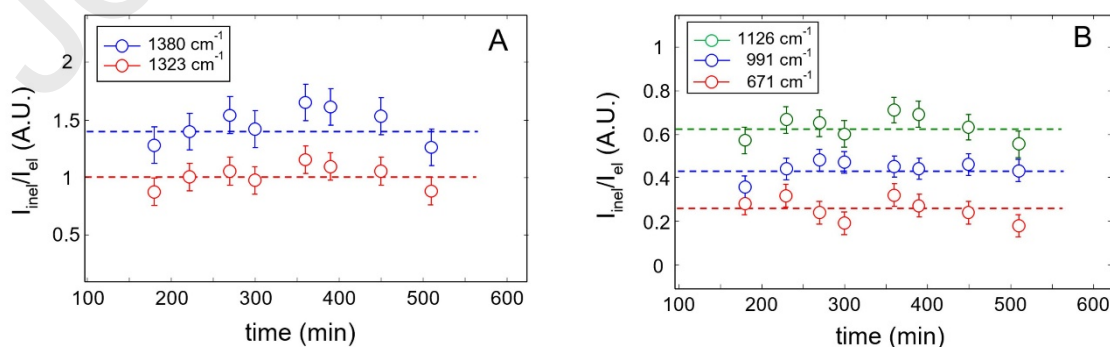


**Figure 8.** Normalized intensity of 6-MP peaks as a function of time. Peak frequencies as indicated. Dotted lines represent the average values of the normalized intensity. Data from the kinetic experiment of Fig. 4.

Fig. 8 illustrates the normalization procedure applied to the kinetic data of Fig. 4. The peak at 1380  $\text{cm}^{-1}$ , which displays a temporal change of more than 20,000 counts, i.e., 550 % of its initial value, after elastic scattering normalization remains essentially constant, with values tightly and randomly distributed around an average figure of 1.48. Thus, the estimated coefficients of variation, CV, (the ratio of the standard deviation to the mean) changes from 64.1 % for the as collected data to 9.0 % after normalization. The hot-spot normalization approach works equally well for other analytical peaks of 6-PM. This is illustrated in Figs. 8A-B for the features at 1323, 1126, 991 and 671  $\text{cm}^{-1}$ .

Fig. 9 displays the intensity vs concentration diagram relative to the peak at 1380  $\text{cm}^{-1}$ . In the 1 – 15  $\mu\text{M}$  range a satisfactory linear correlation is found, represented by the equation:  $I_{1380}^N = 0.094 \cdot C_{6-MP}$ , where  $I_{1380}^N$  is the normalized intensity of the analytical peak and  $C_{6-MP}$  is the analyte concentration in  $\mu\text{mol/L}$ . The correlation coefficient,  $R^2 = 0.921$ , confirms on quantitative grounds the validity of eq.2, the soundness of the proposed normalization approach and identifies a concentration interval within which it is possible to perform quantitation with high accuracy and reproducibility. The  $I_{1380}^N$  value of the 20  $\mu\text{M}$  composition lies below the linearly extrapolated value, setting the upper boundary of the working range. This effect is possibly related to the fact that this composition approaches the saturation limit of the present SERS platform (26  $\mu\text{M}$ ) [26]. In principle, it could be possible to extend the linearity range by increasing the AuNPs concentration, but we have observed that, in doing so the aggregation tends to become faster and less controlled. The error bars in Fig. 9 represent the data scattering of the normalized intensities around the mean for measurements taken at different times. Relative Standard deviations range from 7.7 at 20  $\mu\text{M}$  to 38.3 % at 1.0  $\mu\text{M}$  and are consistently lower than those reported in [40] for 6-MP detection on a 2D plasmonic substrate.

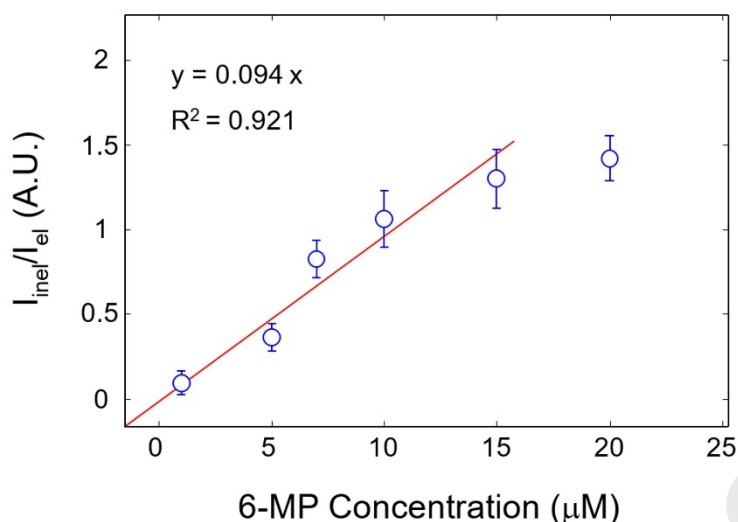


**Figure 9.** Normalized Intensity of the SERS signal at  $1380\text{ cm}^{-1}$  as a function of the concentration of the analyte solution.

The limit of detection (LOD), defined as the analyte concentration producing a signal three times larger than the random noise [41] is heavily dependent, for the present platform, on the time lag between analyte injection and data collection and, therefore, is not easily quantified. For instance, the  $1.0\text{ }\mu\text{M}$  solution goes undetected after 1h, produces a signal just above the LOD after 3 h (SNR = 3.3 at  $1259\text{ cm}^{-1}$ ) and 8.1 times over the LOD after 6 hours (SNR = 24.2). Well-detectable analyte signatures have been identified at  $100\text{ nM}$  concentration (*cf* Fig. S4, Supplementary information): after 6 h the intensity of the  $1259\text{ cm}^{-1}$  peak is 3.3 times larger than the LOD (SNR = 9.8).

The linearity range identified in the present study has been compared with concentration ranges relevant in clinical practice to verify the potential application of the proposed platform in TDM. The pharmacokinetics of 6-MP by intravenous administration to ALL pediatric patients has been reported [42]. Immediately after the administration the concentration of 6-MP in plasma was  $107\text{ }\mu\text{M}$ . It decreased rapidly to  $25.6\text{ }\mu\text{M}$  by completion of the infusion and dropped progressively in the range  $20 - 1\text{ }\mu\text{M}$  in the following 9 h. After 24 h it was undetectable. In another study, the physiological concentration of 6-MP was reported to vary between 100 and  $1\text{ }\mu\text{M}$  [28]. It is concluded that the range of 6-MP concentration exhibiting a linear response function matches well blood concentrations of clinical interest. The linearity range of the present platform is considerably improved in terms of TDM applications, with respect to that reported in [40], which was limited to the  $0.5 - 3.0\text{ }\mu\text{M}$  interval. In terms of LOD, a few competing techniques are still more sensitive ( $0.03\text{ }\mu\text{M}$  by HPLC/UV [42],  $0.06\text{ }\mu\text{M}$  by voltammetry [43]) but in the present case the primary objective was the accuracy of quantitation, rather than the sensitivity. Moreover, the lower limit of the therapeutic window is

around 1.0  $\mu\text{M}$  [44]. In principle, the sensitivity of the present platform can be further improved by using specific nanoparticle morphologies; work is in progress in our laboratories along this line.

It is explicitly noted that in a complex system as the blood plasma, interfering effects may arise from the mixture components, in particular the protein fraction, which could interact with the target molecule and/or compete toward adsorption sites. These effects might alter the detection limits and the linearity ranges. Work is in progress to elucidate this point by extending the present approach to blood plasma samples.

The sensing platform proposed herein provides several benefits: it is sufficiently sensitive for the intended application, is accurate and is designed to reduce drastically instrumental facilities and related laboratory equipment. It requires minimum skills from operating personnel: essentially, it consists in mixing the sensing and the sample solutions, keeping the mixture at room temperature under mild stirring for a prescribed amount of time, and taking the measurement. The data analysis can be readily implemented in a dedicated software package. These advantages, combined with a minimal need for sample pretreatment, the reduced cost of routine Raman instruments and the potential for on-site deployment, make this assaying method a well suited option for TDM and for analyses to be performed at or close to the bedside (Point of Care Tests, POCT).

#### 4. Concluding remarks

In the present study a SERS platform based on a colloidal solution of gold nanoparticles has been optimized for the detection of 6-mercaptopurine. The aim was to implement an assaying method suitable for Therapeutic Drug Monitoring. A kinetic analysis was performed at different analyte concentrations to investigate the complex adsorption/aggregation processes controlling the SERS response of the system. The results allowed us to identify the best conditions for an accurate and reproducible quantitative analysis.

The following conclusions were drawn:

- Adjusting the ionic strength of the solution by HCl addition allowed a sensitivity increment of one order of magnitude with respect to the pristine colloidal solution.
- The increase in sensitivity is due to nanoparticle aggregation with consequent formation of *hot-spots*. The same process causes the precipitation of the larger aggregates at longer times, with loss of SERS activity.

- A normalizing procedure based on the enhanced elastic scattering signal is proposed to minimize the large time-dependence of the analytical signals, so as to obtain a linear correlation of the SERS activity with the analyte concentration.
- A linearity range was identified between 1 and 15  $\mu\text{M}$ , in which it is possible to perform the quantitative analysis with good accuracy and reproducibility. The limiting sensitivity (LOD) of the present platform is 0.1  $\mu\text{M}$ . The linearity range of the present assaying platform is suitable for clinical applications and improves previously reported results.
- The advantages of the present sensing platform (accuracy, low cost, simplicity, easy on-site deployment) make it a viable option for TDM and for Point of Care Tests.

**Acknowledgements:** Thanks are due to Mr. G. Orefice for assistance in the SERS/Raman experiments. We acknowledge the National Research Council of Italy (CNR) for supporting the present project by ordinary funding.

## References

- [1] M.V. Relling, M.L. Hancock, J.M. Boyett, C.-H. Pui, W.E. Evans, Prognostic Importance of 6-Mercaptopurine Dose Intensity in Acute Lymphoblastic Leukemia, *Blood*, 93 (1999) 2817-2823.
- [2] S. Sahasranaman, D. Howard, S. Roy, Clinical pharmacology and pharmacogenetics of thiopurines, *European journal of clinical pharmacology*, 64 (2008) 753-767.
- [3] J.B. Andersen, C. Szumlanski, R. Weinshilboum, K. Schmiegelow, Pharmacokinetics, dose adjustments, and 6-mercaptopurine/ methotrexate drug interactions in two patients with thiopurine methyltransferase deficiency, *Acta Paediatrica*, 87 (1998) 108-111.
- [4] L. Lennard, The clinical pharmacology of 6-mercaptopurine, *European journal of clinical pharmacology*, 43 (1992) 329-339.
- [5] J.S. Kang, M.H. Lee, Overview of therapeutic drug monitoring, *Korean J Intern Med*, 24 (2009) 1-10.
- [6] L. Alnaim, Therapeutic drug monitoring of cancer chemotherapy, *J Oncol Pharm Pract*, 13 (2007) 207-221.
- [7] S.W. Pugh, G. Stocco, W.E. Evans, Pharmacogenomics in pediatric leukemia, *Curr Opin Pediatr*, 22 (2010) 703-710.
- [8] R.H. Larsen, L.L. Hjalgrim, K. Grell, K. Kristensen, L.G. Pedersen, E.D. Brünner, B. Als-Nielsen, K. Schmiegelow, J. Nersting, Pharmacokinetics of tablet and liquid formulations of oral 6-mercaptopurine in children with acute lymphoblastic leukemia, *Cancer Chemotherapy and Pharmacology*, 86 (2020) 25-32.

- [9] S. Supandi, Y. Harahap, H. Harmita, R. Andalusia, Simultaneous Analysis of 6-Mercaptopurine, 6-Methylmercaptopurine, and 6-Thioguanosine-5'-monophosphate in Dried Blood Spot Using Ultra Performance Liquid Chromatography Tandem Mass Spectrometry, 2018, 18 (2018) 8.
- [10] T.L. Ding, L.Z. Benet, Determination of 6-mercaptopurine and azathioprine in plasma by high-performance liquid chromatography, *Journal of Chromatography B: Biomedical Sciences and Applications*, 163 (1979) 281-288.
- [11] Y. Su, Y.Y. Hon, Y. Chu, M.E.C. Van de Poll, M.V. Relling, Assay of 6-mercaptopurine and its metabolites in patient plasma by high-performance liquid chromatography with diode-array detection, *Journal of Chromatography B: Biomedical Sciences and Applications*, 732 (1999) 459-468.
- [12] S. Diamai, W. Warjri, D. Saha, D.P.S. Negi, Sensitive determination of 6-mercaptopurine based on the aggregation of phenylalanine-capped gold nanoparticles, *Colloids and Surfaces A: Physicochemical and Engineering Aspects*, 538 (2018) 593-599.
- [13] Y. Sato, Y. Ishikawa, H. Matsuura, K. Uosaki, F. Mizutani, O. Niwa, Highly-Sensitive Determination of 6-Mercaptopurine and Its Metabolites by Electrochemical Reductive Desorption Measurements, *Electroanalysis*, 17 (2005) 965-968.
- [14] P. Zhou, L. He, G. Gan, S. Ni, H. Li, W. Li, Fabrication and evaluation of [Co(phen)<sub>2</sub>L]<sub>3</sub><sup>+</sup>-modified DNA-MWCNT and SDS-MWCNT electrodes for electrochemical detection of 6-mercaptopurine, *Journal of Electroanalytical Chemistry*, 665 (2012) 63-69.
- [15] M. Keyvanfard, V. Khosravi, H. Karimi-Maleh, K. Alizad, B. Rezaei, Voltammetric determination of 6-mercaptopurine using a multiwall carbon nanotubes paste electrode in the presence of isoprenaline as a mediator, *Journal of Molecular Liquids*, 177 (2013) 182-189.
- [16] Y.-J. Hu, Y. Liu, W. Jiang, R.-M. Zhao, S.-S. Qu, Fluorometric investigation of the interaction of bovine serum albumin with surfactants and 6-mercaptopurine, *Journal of Photochemistry and Photobiology B: Biology*, 80 (2005) 235-242.
- [17] M. Chrzanowska, A. Sloderbach, Spectrophotometric determination of 6-mercaptopurine and 6-thiouric acid by means of induced iodine-azide reaction, *Chemia Analityczna*, 42 (1997) 381-386.
- [18] A. Jaworska, S. Fornasaro, V. Sergio, A. Bonifacio, Potential of Surface Enhanced Raman Spectroscopy (SERS) in Therapeutic Drug Monitoring (TDM). A Critical Review, *Biosensors*, 6 (2016) 47.
- [19] M. Tommasini, C. Zanchi, A. Lucotti, A. Bombelli, N.S. Villa, M. Casazza, E. Ciusani, U. de Grazia, M. Santoro, E. Fazio, F. Neri, S. Trusso, P.M. Ossi, Laser-Synthesized SERS Substrates as Sensors toward Therapeutic Drug Monitoring, *Nanomaterials*, 9 (2019) 677.
- [20] C.M. Coyle, *Surface-Enhanced Vibrational Spectroscopy By Ricardo Aroca* (University of Windsor, Canada). John Wiley & Sons, Ltd: Chichester. 2006. xxvi + 234 pp. \$130. ISBN 0-471-60731-2, *J Am Chem Soc*, 128 (2006) 16411-16411.
- [21] E. Le Ru, P. Etchegoin, *Principles of Surface-Enhanced Raman Spectroscopy: And Related Plasmonic Effects*, Elsevier, Oxford. UK, 2008.
- [22] A. Bonifacio, S. Cervo, V. Sergio, Label-free surface-enhanced Raman spectroscopy of biofluids: fundamental aspects and diagnostic applications, *Analytical and Bioanalytical Chemistry*, 407 (2015) 8265-8277.



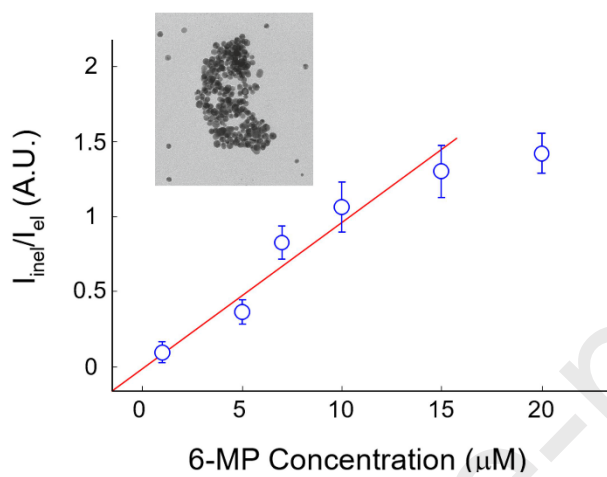
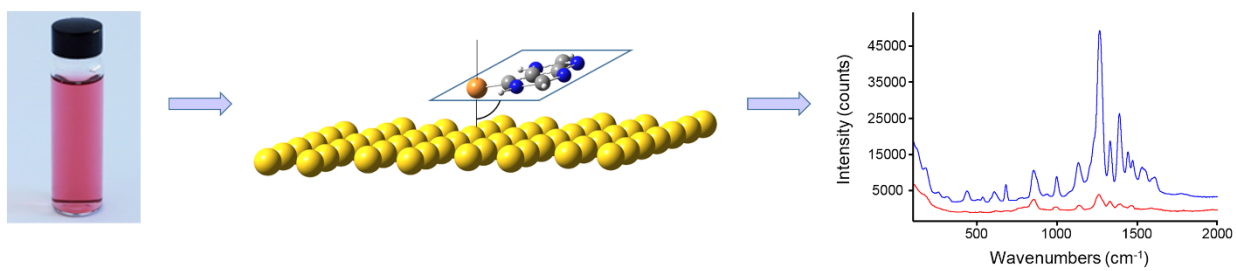
- [23] S. Fornasaro, F. Alsamad, M. Baia, L.A.E. Batista de Carvalho, C. Beleites, H.J. Byrne, A. Chiadò, M. Chis, M. Chisanga, A. Daniel, J. Dybas, G. Eppe, G. Falgayrac, K. Faulds, H. Gebavi, F. Giorgis, R. Goodacre, D. Graham, P. La Manna, S. Laing, L. Litti, F.M. Lyng, K. Malek, C. Malherbe, M.P.M. Marques, M. Meneghetti, E. Mitri, V. Mohaček-Grošev, C. Morasso, H. Muhamadali, P. Musto, C. Novara, M. Pannico, G. Penel, O. Piot, T. Rindzevicius, E.A. Rusu, M.S. Schmidt, V. Sergo, G.D. Sockalingum, V. Untereiner, R. Vanna, E. Wiercigroch, A. Bonifacio, Surface Enhanced Raman Spectroscopy for Quantitative Analysis: Results of a Large-Scale European Multi-Instrument Interlaboratory Study, *Anal Chem*, 92 (2020) 4053-4064.
- [24] M. Pannico, A. Calarco, G. Peluso, P. Musto, Functionalized gold nanoparticles as biosensors for monitoring cellular uptake and localization in normal and tumor prostatic cells, *Biosensors*, 8 (2018) 87.
- [25] E.C. Le Ru, E. Blackie, M. Meyer, P.G. Etchegoin, Surface Enhanced Raman Scattering Enhancement Factors: A Comprehensive Study, *The Journal of Physical Chemistry C*, 111 (2007) 13794-13803.
- [26] M. Pannico, P. Musto, SERS spectroscopy for the therapeutic drug monitoring of the anticancer drug 6-Mercaptopurine: Molecular and kinetic studies, *Applied Surface Science*, 539 (2021) 148225.
- [27] A.J. Viudez, R. Madueño, T. Pineda, M. Blázquez, Stabilization of Gold Nanoparticles by 6-Mercaptopurine Monolayers. Effects of the Solvent Properties, *The Journal of Physical Chemistry B*, 110 (2006) 17840-17847.
- [28] A. Szeghalmi, L. Leopold, S. Pinzaru, V. Chis, I. Silaghi-Dumitrescu, M. Schmitt, J. Popp, W. Kiefer, Adsorption of 6-mercaptopurine and 6-mercaptopurine riboside on silver colloid: a pH dependent surface enhanced Raman spectroscopy and density functional theory study. Part I. 6-Mercaptopurine, *J Mol Struct*, 735 (2005) 103-113.
- [29] H. Chu, H. Yang, S. Huan, G. Shen, R. Yu, Orientation of 6-Mercaptopurine SAMs at the Silver Electrode as Studied by Raman Mapping and in Situ SERS, *The Journal of Physical Chemistry B*, 110 (2006) 5490-5497.
- [30] A. Vivoni, S.-P. Chen, D. Ejeh, C.M. Hosten, Determination of the Orientation of 6-Mercaptopurine Adsorbed on a Silver Electrode by Surface-Enhanced Raman Spectroscopy and Normal Mode Calculations, *Langmuir*, 16 (2000) 3310-3316.
- [31] A. Tripathi, E.D. Emmons, S.D. Christesen, A.W. Fountain III, J.A. Guicheteau, Kinetics and reaction mechanisms of thiophenol adsorption on gold studied by surface-enhanced Raman spectroscopy, *The Journal of Physical Chemistry C*, 117 (2013) 22834-22842.
- [32] B.M. DeVetter, P. Mukherjee, C.J. Murphy, R. Bhargava, Measuring binding kinetics of aromatic thiolated molecules with nanoparticles via surface-enhanced Raman spectroscopy, *Nanoscale*, 7 (2015) 8766-8775.
- [33] R.J. Hunter, *Foundations of Colloid Science*, Clarendon Press, Oxford, UK, 1989.
- [34] P. Alonso-González, P. Albella, M. Schnell, J. Chen, F. Huth, A. García-Etxarri, F. Casanova, F. Golmar, L. Arzubia, L.E. Hueso, J. Aizpurua, R. Hillenbrand, Resolving the electromagnetic mechanism of surface-enhanced light scattering at single hot spots, *Nature Communications*, 3 (2012) 684.
- [35] W. Nam, Y. Zhao, J. Song, S. Ali Safiabadi Tali, S. Kang, W. Zhu, H.J. Lezec, A. Agrawal, P.J. Vikesland, W. Zhou, Plasmonic Electronic Raman Scattering as Internal Standard for Spatial and Temporal Calibration in Quantitative Surface-Enhanced Raman Spectroscopy, *The Journal of Physical Chemistry Letters*, 11 (2020) 9543-9551.

- [36] H. Wei, W. Leng, J. Song, M.R. Willner, L.C. Marr, W. Zhou, P.J. Vikesland, Improved quantitative SERS enabled by surface plasmon enhanced elastic light scattering, *Anal Chem*, 90 (2018) 3227-3237.
- [37] M.Y. Chan, W. Leng, P.J. Vikesland, Surface-Enhanced Raman Spectroscopy Characterization of Salt-Induced Aggregation of Gold Nanoparticles, *ChemPhysChem*, 19 (2018) 24-28.
- [38] P. Gao, M.J. Weaver, Metal-adsorbate vibrational frequencies as a probe of surface bonding: halides and pseudohalides at gold electrodes, *The Journal of Physical Chemistry*, 90 (1986) 4057-4063.
- [39] J.-W. Park, J.S. Shumaker-Parry, Structural Study of Citrate Layers on Gold Nanoparticles: Role of Intermolecular Interactions in Stabilizing Nanoparticles, *J Am Chem Soc*, 136 (2014) 1907-1921.
- [40] L. Zhang, H. Li, G. Chu, L. Luo, J. Jin, B. Zhao, Y. Tian, Detection of 6-Mercaptopurine by silver nanowires-coated silicon wafer based on surface-enhanced Raman scattering spectroscopy, *Colloids and Surfaces A: Physicochemical and Engineering Aspects*, 508 (2016) 309-315.
- [41] S. Schlucker, *Surface Enhanced Raman Spectroscopy. Analytical, Biophysical and Life Science Applications*, WILEY-VCH Verlag & Co., Weinheim, Germany, 2011.
- [42] E. Jacqz-Aigrain, S. Nafa, Y. Medard, E. Bessa, B. Lescoeur, E. Vilmer, Pharmacokinetics and distribution of 6-mercaptopurine administered intravenously in children with lymphoblastic leukaemia, *European journal of clinical pharmacology*, 53 (1997) 71-74.
- [43] A.A. Ensafi, H. Karimi-Maleh, Determination of 6-mercaptopurine in the presence of uric acid using modified multiwall carbon nanotubes-TiO<sub>2</sub> as a voltammetric sensor, *Drug testing and analysis*, 4 (2012) 970-977.
- [44] R.H. Larsen, L.L. Hjalgrim, K. Grell, K. Kristensen, L.G. Pedersen, E.D. Br nner, B. Als-Nielsen, K. Schmiegelow, J. Nersting, Pharmacokinetics of tablet and liquid formulations of oral 6 - mercaptopurine in children with acute lymphoblastic leukemia, *Cancer Chemotherapy and Pharmacology*, (2020).

**Credit author statement**

The authors contributed equally to the present study.

Journal Pre-proofs



**Research Highlights**

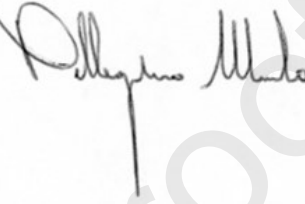
- A SERS colloidal solution of gold nanoparticles is proposed as a sensing platform potentially suitable for the Therapeutic Drug Monitoring of the anticancer drug 6-mercaptopurine.
- The platform sensitivity was enhanced by one order of magnitude adjusting the pH of the colloidal solution toward acidic values.
- A normalization approach allowed us to remove the time-dependence of the SERS signal and to identify a linearity range suitable for clinical applications.

Journal Pre-proofs

## Declaration of Competing Interest

The authors declare that they have no known competing financial interests or personal relationships that could have appeared to influence the work reported in this paper.

Pellegrino Musto

A handwritten signature in black ink that reads "Pellegrino Musto". The signature is written in a cursive style with a long vertical line extending downwards from the end of the name.

Journal Pre-proofs